SUPPLEMENTARY INFORMATION

Effects of *ex vivo* blood anticoagulation and preanalytical processing time on the proteome content of platelets

Samuel Tassi Yunga[1,2*], Austin J. Gower[1], Alexander R. Melrose[3], Meghan K. Fitzgerald[1], Ashmitha Rajendran[1], Theresa A. Lusardi[1], Randall J. Armstrong[1], Jessica Minnier[1,3], Kelley R. Jordan[2], Owen J. T. McCarty[2], Larry L. David[4,5], Phillip A. Wilmarth[4], Ashok P. Reddy[4], and Joseph E. Aslan[2,3,5*]

[1]Cancer Early Detection Advanced Research Center (CEDAR), Knight Cancer Institute, School of Medicine; [2]Department of Biomedical Engineering, School of Medicine; [3]Knight Cardiovascular Institute, Division of Cardiology, School of Medicine; [4]Proteomics Shared Resource; [5]Department of Chemical Physiology & Biochemistry, School of Medicine; Oregon Health & Science University, 3181 SW Sam Jackson Park Road, Portland, OR 97239; USA

*Correspondence to: Samuel Tassi Yunga, M.D., Ph.D.
Oregon Health & Science University
2720 S Moody Avenue
Portland, OR 97201; U.S.A.
Email: tassiyun@ohsu.edu

Joseph Aslan, Ph.D.
Oregon Health & Science University
3303 SW Bond Ave.
Portland, OR 97239; U.S.A.
Email: aslanj@ohsu.edu
Twitter: @JoePlatelet

Supplemental Methods

Platelet-platelet aggregation in PRP

Immediately prior to aggregation assays (t=0), platelet counts in PRP were estimated by flow cytometry and then normalized to 5 x 10^7 platelets/ml by diluting PRP into matched PPP. To enumerate platelets, a 50 µl aliquot of each unstained PRP sample was mixed with 950 µl of PBS and 10 µl of CountBright Absolute Counting Beads (Thermo Fisher Scientific # C36950), and analyzed on a BD FACSymphony instrument, as detailed below. Platelet concentration was calculated based on the number of bead events and platelet events per 1 min acquisition, the known bead concentration and the dilution factor of PRP. Platelet aggregation was assessed through spectrophotometric measurements of PRP turbidity as previously described [1]. In brief, 90 µl of PRP was transferred into triplicate wells of clear/flat-bottom 96-well plates, followed by addition of 10 µl of control buffer (PBS) or 10 µl of platelet agonist (20 µM TRAP6 or 10 µg/ml of crosslinked collagen-related peptide CRP-XL). Plates were immediately loaded in a TECAN Spark 20M microplate reader and monitored in real time at 37ºC for changes in absorbance at 650 nm, over 30 min (20 cycles), with gentle orbital shaking preceding each cycle. The percent platelet aggregation (or % light transmission) was assessed as a decrease in absorbance (increase in light transmission) over time, where the initial PRP absorbance was considered as 0% aggregation and the absorbance of PPP control samples as 100% aggregation at each cycle.

Complete blood counts

Erythrocyte count, leukocyte count, platelet count, mean platelet volume (MPV) and other parameters were determined in differentially anticoagulated blood samples from three donors, approximately 1 h after blood draw. Hematology assays were carried out by CLIA-certified OHSU Laboratory Services. Raw platelet counts in blood from ACD and NaCit tubes were adjusted for anticoagulant dilution before data analysis. The plateletcrit (PCT) was calculated by multiplying the platelet count by MPV.

Flow cytometry analysis of platelet activation and monocyte-platelet aggregation

Anticoagulated blood (5 µl) from each time point were transferred into 5 ml Falcon tubes containing 85 µl of HEPES/Tyrode (H-T) buffer (129 mM NaCl, 20 mM HEPES, 12 mM $NaHCO_3$, 2.9 mM KCl, 1 mM $MgCl_2$, 0.34 mM $Na_2HPO_4 \bullet 12H_2O$ and 5 mM D-glucose, pH 7.3) and 10 µl antibody cocktail, to a final volume of 100 µl. Antibodies used for different cocktails included CD41a-BV421 (HIP8, Biolegend #303730), CD62P-APC (AK4, Biolegend #304910), CD45-BUV395 (HI30, BD #563792), CD14-PE-Cy7 (M5E2, BD #557742), CD63-AF647 (H5C6, Biolegend #353016) and CD61-AF647 (VI-PL2, BioLegend # 336408), each at a 1:40 final dilution. The reaction mix was incubated for 15 min (rt, 200 rpm). Stained samples were then fixed in 1% paraformaldehyde (PFA) and diluted in for flow cytometry analysis. CountBright Absolute Counting Beads (10 µl of stock with known concentration) were added to the solution before analysis on a BD FACSymphony instrument equipped with 200 mW 405 nm, 488 nm, 561 nm, and 640 nm lasers. The flow cytometer was calibrated daily with CS&T beads (BD #656505) to ensure proper laser alignment and instrument performance. The trigger threshold was set at 200 (FSC), window extension at 10, and total acquisition time of 150 s at low pressure. Compensation was performed using OneComp eBeads (Thermo # 01-1111-42) stained with the same antibodies as test samples. A platelet activation positive control sample was included by adding the agonist TRAP6 during blood staining at a final concentration of 10 µM. Gating schemes for platelets ($CD41a^+$), monocyte platelet aggregates ($CD45^+CD14^+CD41a^+$), P-selectin positive platelets ($CD41a^+CD62P^+$, α-granule secretion), CD63-positive platelets ($CD41a^+CD63^+$, dense granule secretion) are shown in **S. Fig. S3A**.

Nanoscale flow cytometry analysis of platelet extracellular vesicle release

Prior to analyzing the anticoagulant-induced release of extracellular vesicles (EVs) from platelets, instrument and assay optimization was performed to enable reproducible detection and quantification of nanoscale (50-1000 nm), membrane-enclosed (detergent-labile) events with minimal coincidence, optimal signal-to-noise separation and low background fluorescence (**S. Fig. S4A-G**). With the optimized conditions, platelet-derived EVs (defined herein as $CD41a^+CD9^+$), were analyzed in 2,500 × *g* -spun PPP prepared from blood anticoagulated with ACD, NaCit, EDTA and heparin for 1, 2, 3, 5, 9, 24, 48 and 120 h. The PPP samples (pre-diluted

1/10 in 0.1 μm-filtered PBS) and antibodies (CD41a-BV421 – HIP8, Biolegend #303730; and CD9-PE – HI9a, Biolegend #312105, also prediluted 1/10 in filtered PBS) were combined at a ratio of 9 μl:1 μl and incubated overnight (4°C, 200 rpm). Stained samples were further diluted in filtered PBS before analysis on a BD FACSymphony instrument equipped with a High Throughput Sampler (HTS) system for auto-sampling of all test samples from a 96-well plate. The concentration of $CD41a^+CD9^+$ platelet EVs in each PPP sample was estimated based on the number of events acquired in 60s, the acquisition flow rate (1 μl/s) and the total PPP dilution factor including additional adjustments for dilution of blood in liquid citrated anticoagulants.

Western blotting

Platelets were lysed in Laemmli buffer with 0.2M DTT, separated by SDS-PAGE and transferred onto PVDF membranes. After blocking in 5% BSA, membranes were probed with primary antibodies overnight at 4°C, washed with TBS-T and incubated with corresponding secondary antibodies. Blots were developed and digitally scanned as previously described [2]. Primary antibodies included FCN3 (R&D Systems, MAB2367), C1R (Invitrogen/ThermoFisher, PA5-28028), MPO (R&D Systems, AF3667), and α-tubulin (Sigma, T6199).

Multiplex plasma protein profiling by Luminex assay

A custom premixed Luminex multianalyte kit (R&D Systems) was used to measure proteins in plasma, including PPBP, PF4, SPARC, SERPINE1, RANTES, VEGFC, TIMP1 and MPO. In brief, PPP and kit standards were incubated with an antibody-coated magnetic microparticle cocktail for 2 h at rt. After washing the microparticles on a microplate magnet, a biotin-antibody cocktail was added for 1 h followed by more wash cycles and incubation in streptavidin-PE for 30 min. The microparticles were washed again and resuspended in 100 μl of wash buffer and read on a Luminex 200 system. The instrument was programmed to read 50 microparticle counts per analyte region, with a doublet discriminator gate setting of 8,000-16,500. Blank median fluorescence intensity (MFI) values were subtracted from sample MFIs and plasma concentrations in pg/ml were calculated using five-parameter logistic (5-PL) standard curves.

Concentrations were adjusted for plasma pre-dilution in buffer (1/125 for PF4 and 1/5 for other analytes) and in liquid anticoagulant (only for citrated anticoagulants).

Flow cytometry-based detection of NET products on platelets

Sequestration of neutrophil extracellular trap (NET) components by blood platelets in heparinized blood was verified by a flow cytometry assay that employs a membrane-impermeable DNA-binding dye (SYTOX) and anti-myeloperoxidase (MPO) antibodies [3]. To examine anticoagulant-induced NET formation *in vitro*, 7.5 µl of whole blood was stained with 2 µl CD45-BUV395 (HI30, BD #563792), 2 µl CD66B-BV421 (6/40c BioLegend # 392915), 1 µl MPO-APC (Abcam, #ab225476) and 5nM SYTOX Green (ThermoFisher Scientific # S7020) in H-T buffer (total reaction mix = 100 µl) for 30 min at rt. Stained samples were fixed as above, further diluted to 500 µl and analyzed on a BD FACSymphony. Another assay was performed but replacing the anti-MPO-APC antibody with the anti-neutrophil elastase (ELA2 or ELANE)-AF647 anybody. In both cases, neutrophils were gated by co-expression of CD45 and CD66B. The degree of NET formation was defined as the percent of $CD45^{+}CD66B^{+}$ cells that were positive for both MPO and SYTOX-Green or ELANE and SYTOX-Green respectively. Similar assays were performed for platelets using 30 µl of PRP and replacing the CD66B-BV421 antibody with CD41a-BV421 (HIP8, Biolegend #303730). Pure platelet populations were confirmed by SSC/CD41 gating before assessing for SYTOX-Green/MPO or SYTOX-Green/ELANE co-signals.

TMT labelling

Two sets of 11-plex Tandem Mass Tag (TMT) isobaric reagents (ThermoFisher Scientific) were used to label 18 platelet peptide samples (3 donors × 3 anticoagulants [NaCit+ACD, EDTA, Heparin] × 2 time points [1 h and 24 h]) and 4 technical replicates of internal reference standard (IRS) peptides. The reference standard was made by pooling equal amounts of peptides from all 18 individual samples and dividing into 4 technical replicates as previously described [4-6]. Next, 20 µg of peptide/sample or pooled standard were distributed into channels of TMT-11plex 1 (1 h samples × 9 + 2 pooled reference standards) and TMT-11plex 2 (24 h samples × 9 + 2

reference standards). A preliminary 2 h LC-MS/MS run on an Orbitrap Fusion instrument was performed to check for labelling efficiency and to normalize total reporter ion intensities across channels in each 11-plex. The normalization factors were used to determine the volume ratios needed to constitute a 50 µg mix of each plex in preparation for LC-MS/MS.

LC-MS/MS and data analysis

Each volume-normalized TMT plex mix was quenched in hydroxylamine (0.5% final), incubated at rt for 15 min and dried in a speedvac. Dried samples were dissolved in 60 µl of 10 mM ammonium formate (pH 9), vortexed for 1 minute, incubated at 37°C for 15 min, centrifuged for 2 min and transferred to autosampler tubes. The samples were injected and fractionated (online RP-RP) into 18 fractions per TMT plex (14%, 17%, 20%, 21%, 22%, 23%, 24%, 25%, 26%, 27%, 28%, 29%, 30%, 35%, 40%, 45%, 50%, 90% ACN with 10 mM ammonium formate pH 10) before mass spectrometry in the Orbitrap Fusion Tribrid mass spectrometer. MS2 scans were performed after collision-induced dissociation (CID) to select fragment ions and higher energy dissociation (HCD) was used to generate reporter ions. A high resolution MS3 scan was used to measure reporter ion height. Data was processed using COMET/PAW pipeline [7, 8] against Uniprot human database and EdgeR to determine the number of unique proteins detected and evaluate proteome changes. The two TMT plexes were combined by internal reference scaling (IRS) using the duplicate reference peptide channels in each plex to enable plex-to-plex relative quantification. The IRS-normalized data was subject to trimmed mean of M values (TMM) normalization to address any sample composition bias. The mass spectrometry proteomics data, Jupyter notebooks, R scripts and other resources are publicly available through the ProteomeXchange Consortium via the PRIDE [9] partner repository with the dataset identifier PXD030225. Data analysis and visualization was also carried out using the START app [10], hosted by Shiny at https://kcvi.shinyapps.io/STARTapp_846/ Gene ontology (GO) and Reactome pathway analyses were carried out in STRING (v11.5) and visualized with Cytoscape (v3.8).

Supplemental Tables

Supplemental Table S1. Complete Blood Count (CBC)

CBC Parameter	Donor	Anticoagulant (1 hour)				ANOVA (Friedman)	Significant comparisons
		ACD	NaCit	EDTA	Heparin		
Platelets, $x10^3/\mu l$ [NR = 150-450]	D1	340	268	345	113	p = 0.002	Heparin< EDTA
	D2	219	196	282	144		
	D3	179	149	198	88		
Mean Platelet Volume (MPV), fL [NR = 9.7-12.3]	D1	8.5	10	9.8	10	p = 0.004	ACD< Heparin. ACD<EDTA
	D2	8.1	8.9	9	10.1		
	D3	10.1	10.5	11.5	12.3		
White Blood Cells, $x10^3/\mu l$ [NR = 3.5-10.8]	D1	5.28	5.25	5.15	5.23	ns	n/a
	D2	5.98	6.62	6.22	6.07		
	D3	4.78	5.18	4.94	4.75		
Lymphocytes, $x10^3/\mu l$ [NR = 1.0-4.8]	D1	1.34	1.35	1.37	1.3	ns	n/a
	D2	2	2.25	2.02	2.08		
	D3	1.81	1.96	1.87	1.82		
Monocytes, $x10^3/\mu l$ [NR = 0.1-0.9]	D1	0.3	0.29	0.26	0.28	ns	n/a
	D2	0.48	0.51	0.48	0.42		
	D3	0.51	0.49	0.5	0.43		
Neutrophil, $x10^3/\mu l$ [NR = 1.8-7.7]	D1	3.53	3.5	3.43	3.53	ns	n/a
	D2	3.25	3.51	3.41	3.24		
	D3	2.3	2.54	2.38	2.34		
Eosinophils, $x10^3/\mu l$ [NR = 0.0-0.5]	D1	0.05	0.04	0.04	0.05	ns	n/a
	D2	0.2	0.24	0.24	0.24		
	D3	0.11	0.13	0.12	0.1		
Basophils, $x10^3/\mu l$ [NR = 0.0-0.1]	D1	0.05	0.06	0.04	0.06	ns	n/a
	D2	0.05	0.07	0.06	0.07		
	D3	0.04	0.04	0.06	0.05		
Red Blood Cells, $x10^6/\mu l$ [NR = 4.5-6.0]	D1	4.16	4.14	4.23	4.23	ns	n/a
	D2	5.33	5.38	5.36	5.41		
	D3	5.2	5.25	5.24	5.32		
Mean Corpuscular Volume (MCV), fL [NR = 80-100]	D1	106.9	96	95.7	93.1	p = 0.009	NaCit< ACD
	D2	93.9	85.6	86	84.3		
	D3	99.3	90.3	91	88.3		

Supplemental Table S2 "*Mass spectrometry quantitation, normalization, and analysis*" is provided as a separate, accompanying .xlsx file (Table_S2.xlsx).

Supplemental Figures

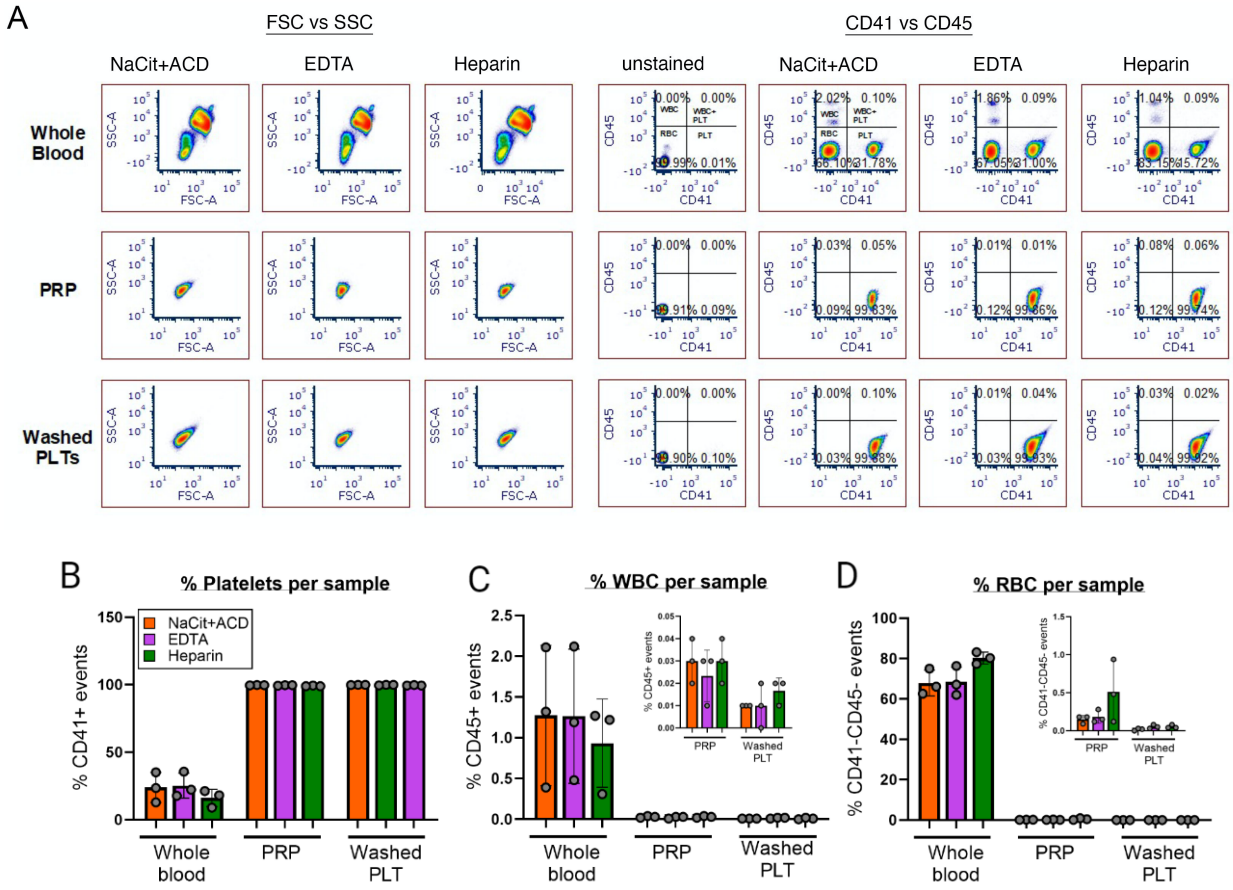

Supplemental Figure S1. Platelet sample purity as determined by flow cytometry analysis. (**A**) Blood cell events for whole anticoagulated blood samples (n=3), platelet rich plasma (PRP) and platelet poor plasma (PPP) preparations are displayed in forward vs side scatter plots and by their expression of CD41 and CD45. Platelets are identified as CD41+CD45- events, and white blood cells (WBC) are identified as CD41-CD45+ events. Red blood cells (RBC) are identified as events negative for both CD41 and CD45 (CD41-CD45- events), with low granularity (low SSC) and low size (low FSC) matching that of other CD235a+ (glycophorin A) events, as described in Babur et al., *Blood* 2020 (4). (**B**) CD41+ events are significantly enriched in PRP and washed platelets (>99% irrespective of anticoagulant). (**C**) WBCs are significantly depleted in PRP and washed platelets, without significant differences across anticoagulants. (**D**) RBC are significantly depleted in washed platelets for all anticoagulant conditions.

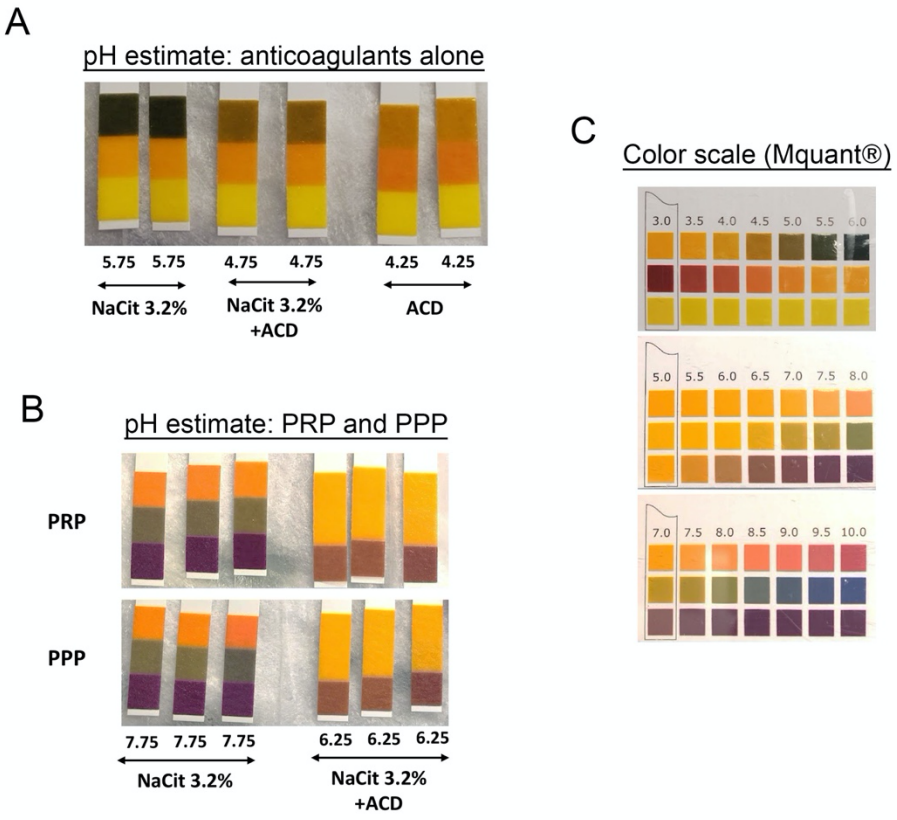

Supplemental Figure S2. Effect of citrate anticoagulant solutions on plasma pH. (A) Before blood draw, solutions of NaCit 3.2% (BD #369714), ACD (25 g/l NaCit, 20 g/l D-glucose, 15 g/l citric acid) and NaCit+ACD (equal volumes) were assessed for pH using MQuant pH-indicator strips (EMD Millipore). (**B**) pH measurements of platelet rich plasma (PRP) and platelet poor plasma (PPP) preparations from NaCit or NaCit+ACD anticoagulated blood samples in **Fig. 1** (n=3). The final plasma composition of anticoagulants were as follows: for NaCit tube (NaCit 3.2 g/l) and for NaCit+ACD tubes (5.7 g/l NaCit, 1.5 g/l citric acid and 2 g/l D-glucose). (**C**) pH values were estimated using a reference color scale.

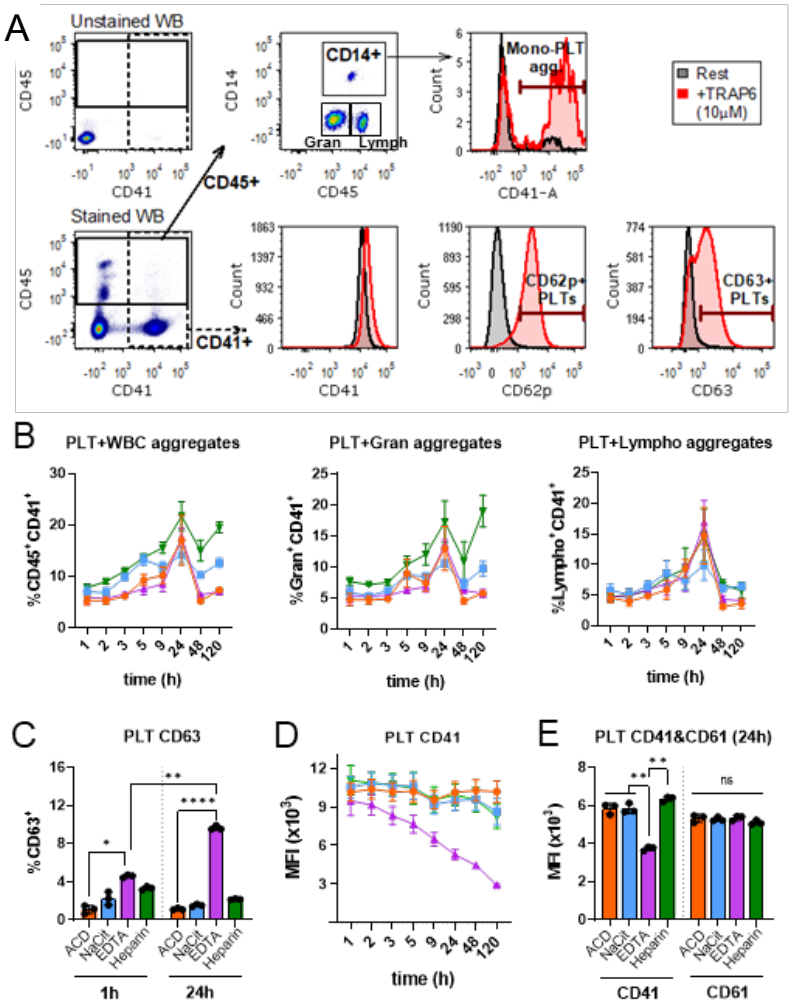

Supplemental Figure S3. Extended flow cytometry evaluation of whole blood for platelet physiological changes during *ex vivo* anticoagulation. (**A**) Gating strategy on the BD FACSymphony instrument. Platelets and white blood cells were gated by CD41a and CD45 expression respectively. Platelet activation with granule release was assessed by surface expression of CD62P and CD63 on $CD41a^{+}$ events. All $CD45^{+}$ events were further segregated into monocytes ($CD14^{+}$) granulocytes ($CD14^{-}CD45^{low}$) and lymphocytes ($CD14^{-}CD45^{high}$). An overlay of plots for TRAP6-treated vs resting whole blood was used to establish gates for activated platelets and white cell populations forming aggregates with platelets. (**B**) Time course analysis of the percent of WBC, granulocyte and lymphocyte events that co-expressed CD41a in differentially anticoagulated blood. (**C**) Increased percent of platelets expressing surface CD63 in EDTA blood at 1 hour and 24 hours after phlebotomy. (**D**) The Median Fluorescence Intensity (MFI) of CD41a on platelet surface membrane steadily dropped over time, exclusively for platelets in blood stored with EDTA anticoagulant. To ensure day-to-day assay reproducibility, the same cytometer settings were used for all days and the MFI stability of control CountBright beads was tracked in the same BV421 channel as the CD41a antibody (bead MFI CV = 2.5%). (**E**) The EDTA-related drop in CD41a MFI was not accompanied by a change in CD61 intensity (time point = 24 hours). Blood samples from 3 healthy donors were used for all experiments.

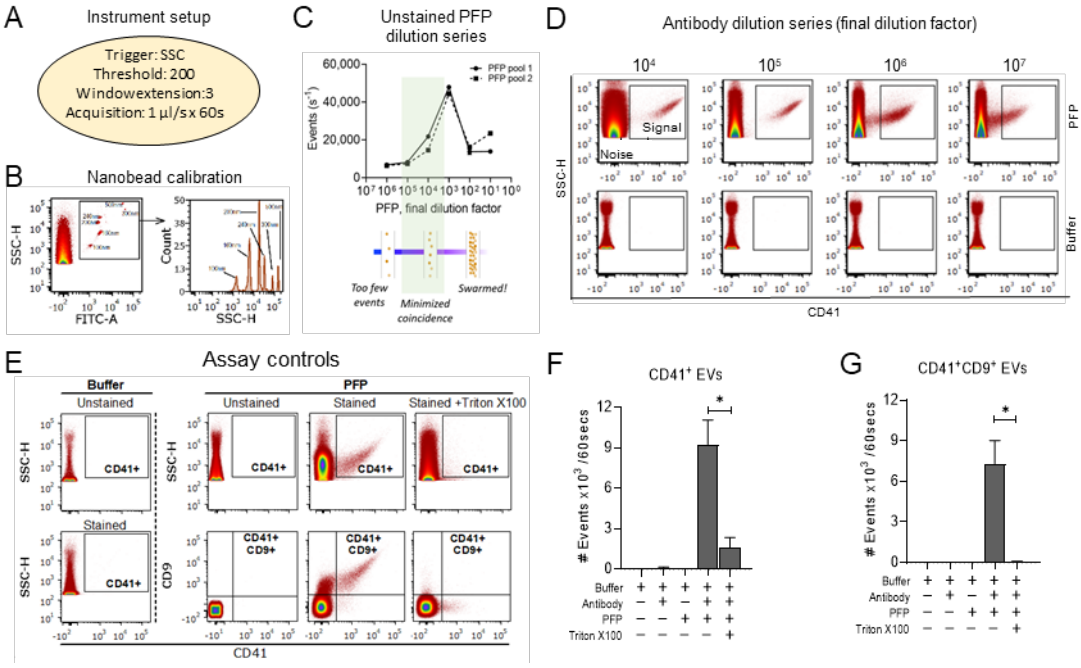

Supplemental Figure S4. **Optimization of nanoscale flow cytometry for detection and quantification of platelet-derived extracellular vesicles.** (**A**) Modified setup parameters on the BD FACSymphony instrument. (**B**) MegaMix nanobeads used for day-to-day instrument calibration and reproducibility check. (**C**) Serial dilution of two unstained platelet-free plasma (PFP) pools to determine optimal dilution range. Event rates increased with plasma concentration from 10^6 to 10^3 PFP dilution and dropped at lower dilutions due to coincidence. (**D**) Antibody dilution series to determine dilution factors with optimal separation of signal from noise. Buffer-only controls detect background fluorescent signals. For CD41a-BV421, a final dilution of 10^4-10^5 gave the best separation of signal from noise with minimal background fluorescence. A similar experiment was performed for CD9-PE (data not shown). (**E**) Gating of events co-expressing CD41a and CD9, defined here as platelets EVs. $CD41a^+CD9^+$ events were absent in unstained PFP and were labile to Triton-X100 detergent treatment confirming they are membrane-enclosed particles. (**F, G**) Quantitative data from panel E (n=3 donor PFP).

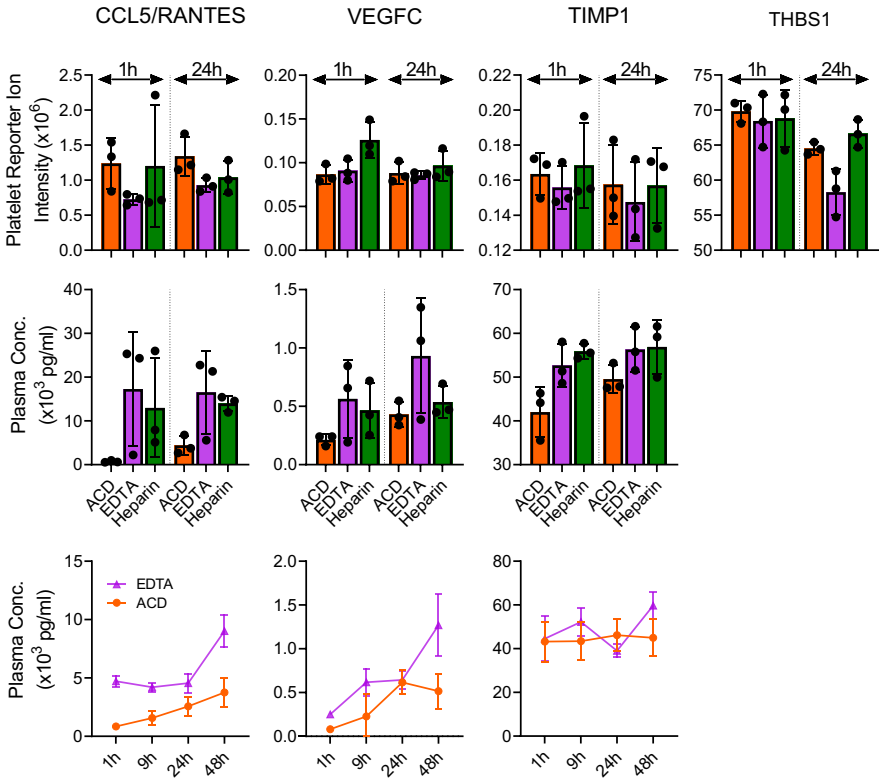

Supplemental Figure S5. EDTA-associated changes in additional platelet alpha granule released proteins. Platelet reporter ion intensity distribution for other representative alpha granule proteins, CCL5, VEGFC, TIMP1 and THBS1 (top row). Levels of the corresponding proteins were also quantified by multiplex bead-based Luminex assay in reciprocal platelet-free plasma after 1 hour and 24 hours of blood storage (middle row) and through 48 hours (lower row, only EDTA vs NaCit+ACD).

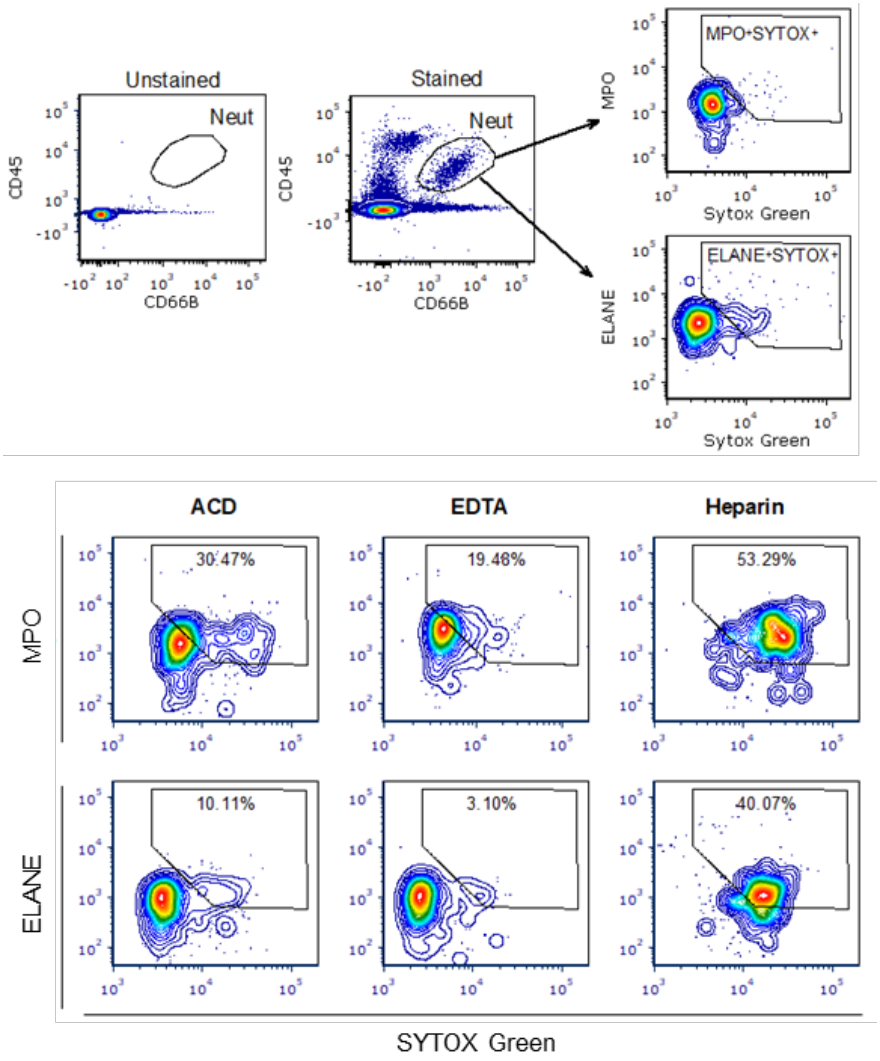

Supplemental Figure S6. Gating NET-forming neutrophils in whole blood. Neutrophils in whole blood were gated by co-expression of CD45 and CD66B. Gated neutrophils were further assessed for surface expression of neutrophil granule enzymes (MPO or ELANE) and extruded DNA (detected using the membrane-impermeable dye SYTOX Green). Co-expression of SYTOX-Green and MPO or SYTOX-Green and ELANE defined NET-forming neutrophils. The percent NET-forming neutrophils was assessed in whole blood anticoagulated with NaCit+ACD, EDTA or heparin.

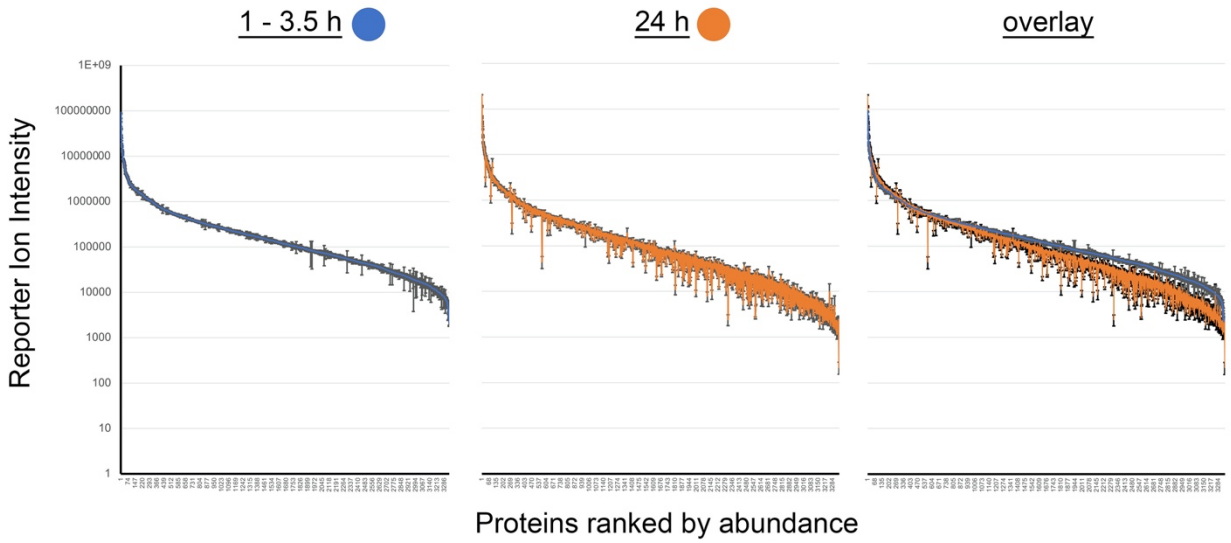

Supplemental Figure S7. Dynamic range and variability of washed platelet proteomes following 1-3.5 h vs 24 h delays in sample processing. *Left*. Summary of mean reporter ion intensity values (blue) for washed human platelet samples (n=10 different healthy human donors), prepared from NaCit+ACD anticoagulated blood following 1-3.5 h delays in processing from our ongoing studies in our group. *Middle*. Mean reporter ion intensity values (orange) for washed human platelet samples from NaCit+ACD anticoagulated blood with 1 h and 24 h delays in processing, as detailed in the main manuscript (n=6; 3 donors, 2 time points). *Right*. Overlay of 1-3.5 h (blue) and 1 vs. 24 h (orange) datasets. Platelet proteins ranked by abundance from left to right on the x-axes (most abundant protein #1=filamin; least abundant protein #3300= MRPL53). Error bars show standard error of mean (SEM).

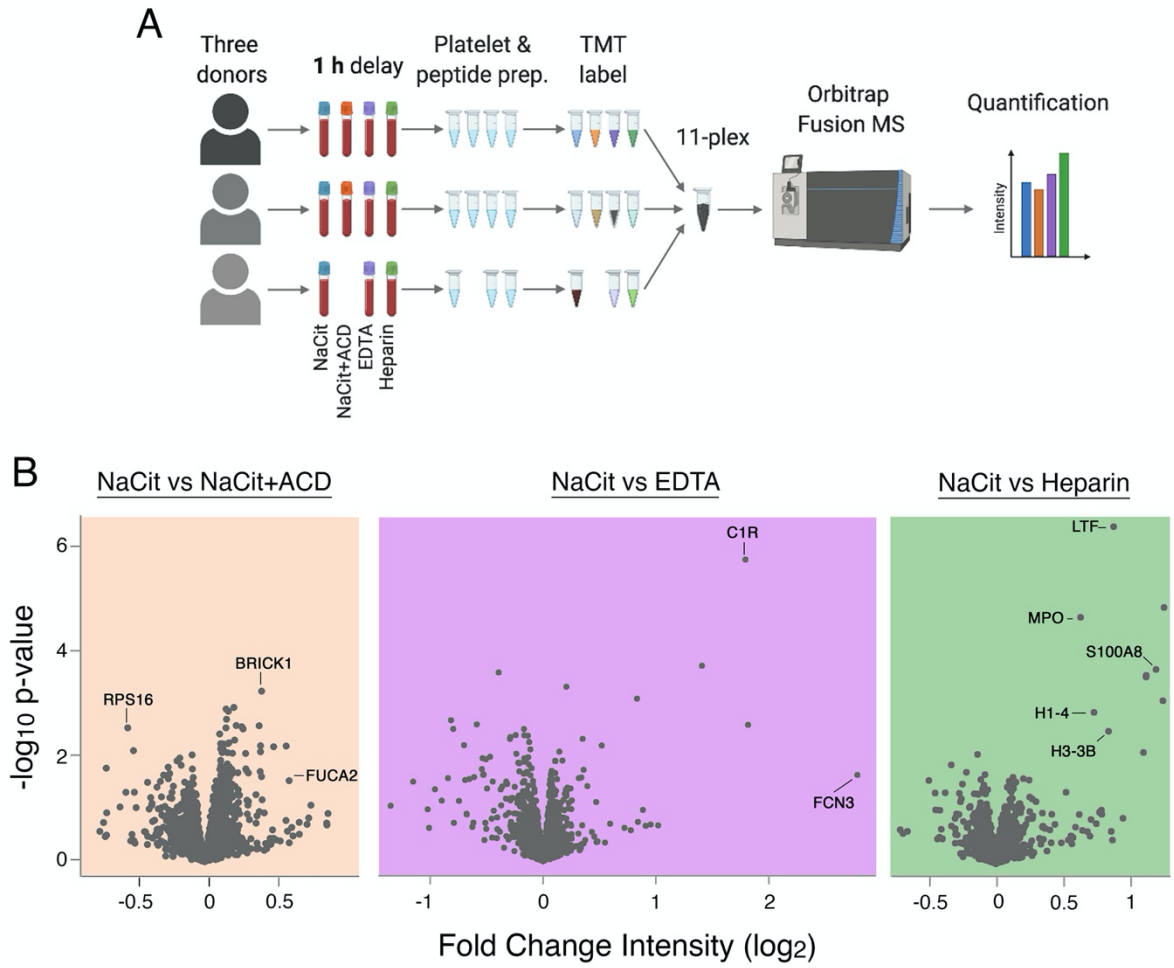

Supplemental Figure S8. Effect of sodium citrate anticoagulation on platelet proteome. (**A**) Experiment design and workflow. A total of 11 washed platelet samples were prepared from blood from n=3 donors × 4 anticoagulant conditions (NaCit, NaCit+ACD, EDTA and Heparin). After 1 h, platelet samples were lysed for tryptic digest, and peptides from each platelet sample were labeled with 11-plex tandem mass tags (TMT). Online fractionation was performed for each before mass spectrometry (MS) in an Orbitrap Fusion Tribrid mass spectrometer. (**B**) Volcano plots of platelet protein reporter ion intensity ratios vs statistical significance, showing two-way comparisons for NaCit vs NaCit+ACD, NaCit vs EDTA and NaCit vs heparin (n=3). No significant differences in platelet proteomes were apparent for NaCit (alone) vs NaCit+ACD conditions. Differences between NaCit (alone) vs EDTA and NaCit (alone) vs heparin preparations were similar to differences between NaCit+ACD sample preparation detailed in the manuscript. Mass spectrometry data, Jupyter notebooks, R scripts and other files for this experiment have been deposited to the ProteomeXchange Consortium via the PRIDE partner repository at Project Accession PXD026903.

Supplemental References

1 Hu CM, Fang RH, Wang KC, Luk BT, Thamphiwatana S, Dehaini D, Nguyen P, Angsantikul P, Wen CH, Kroll AV, Carpenter C, Ramesh M, Qu V, Patel SH, Zhu J, Shi W, Hofman FM, Chen TC, Gao W, Zhang K, Chien S, Zhang L. Nanoparticle biointerfacing by platelet membrane cloaking. *Nature*. 2015; **526**: 118-21. 10.1038/nature15373.

2 Aslan JE, Tormoen GW, Loren CP, Pang J, McCarty OJ. S6K1 and mTOR regulate Rac1-driven platelet activation and aggregation. *Blood*. 2011; **118**: 3129-36. 10.1182/blood-2011-02-331579.

3 Masuda S, Shimizu S, Matsuo J, Nishibata Y, Kusunoki Y, Hattanda F, Shida H, Nakazawa D, Tomaru U, Atsumi T, Ishizu A. Measurement of NET formation in vitro and in vivo by flow cytometry. *Cytometry A*. 2017; **91**: 822-9. 10.1002/cyto.a.23169.

4 Babur O, Melrose AR, Cunliffe JM, Klimek J, Pang J, Sepp AI, Zilberman-Rudenko J, Tassi Yunga S, Zheng T, Parra-Izquierdo I, Minnier J, McCarty OJT, Demir E, Reddy AP, Wilmarth PA, David LL, Aslan JE. Phosphoproteomic quantitation and causal analysis reveal pathways in GPVI/ITAM-mediated platelet activation programs. *Blood*. 2020; **136**: 2346-58. 10.1182/blood.2020005496.

5 Cooper ST, Wilmarth PA, Cunliffe JM, Klimek JE, Pang J, Tassi Yunga S, Minnier J, Reddy A, David LL, Aslan JE. Platelet proteome dynamics in hibernating 13-lined ground squirrels. *Physiol Genomics*. 2021. 10.1152/physiolgenomics.00078.2021.

6 Plubell DL, Wilmarth PA, Zhao Y, Fenton AM, Minnier J, Reddy AP, Klimek J, Yang X, David LL, Pamir N. Extended Multiplexing of Tandem Mass Tags (TMT) Labeling Reveals Age and High Fat Diet Specific Proteome Changes in Mouse Epididymal Adipose Tissue. *Mol Cell Proteomics*. 2017; **16**: 873-90. 10.1074/mcp.M116.065524.

7 Eng JK, Jahan TA, Hoopmann MR. Comet: an open-source MS/MS sequence database search tool. *Proteomics*. 2013; **13**: 22-4. 10.1002/pmic.201200439.

8 Wilmarth PA, Riviere MA, David LL. Techniques for accurate protein identification in shotgun proteomic studies of human, mouse, bovine, and chicken lenses. *J Ocul Biol Dis Infor*. 2009; **2**: 223-34. 10.1007/s12177-009-9042-6.

9 Perez-Riverol Y, Csordas A, Bai J, Bernal-Llinares M, Hewapathirana S, Kundu DJ, Inuganti A, Griss J, Mayer G, Eisenacher M, Perez E, Uszkoreit J, Pfeuffer J, Sachsenberg T, Yilmaz S, Tiwary S, Cox J, Audain E, Walzer M, Jarnuczak AF, Ternent T, Brazma A, Vizcaino JA. The PRIDE database and related tools and resources in 2019: improving support for quantification data. *Nucleic Acids Res*. 2019; **47**: D442-D50. 10.1093/nar/gky1106.

10 Nelson JW, Sklenar J, Barnes AP, Minnier J. The START App: a web-based RNAseq analysis and visualization resource. *Bioinformatics*. 2017; **33**: 447-9. 10.1093/bioinformatics/btw624.